Synthesis and Characterization of a Novel Terthiophene-Based Quinodimethane Bearing a 3,4-Ethylenedioxythiophene Central Unit

Anna Berlin,[†,‡] Sara Grimoldi,[†] Gianni Zotti,[§,||] Reyes Malavé Osuna,[⊥] Mari Carmen Ruiz Delgado,[⊥] Rocío Ponce Ortiz,[⊥] Juan Casado,[⊥] Víctor Hernández,[⊥] and Juan T. López Navarrete*,[⊥]

Istituto CNR di Scienze e Tecnologie Molecolari, via C. Golgi 19, 20133 Milano, Italy, Istituto CNR per L'Energetica e le Interfasi, C.o Stati Uniti 4, 35127 Padova, Italy, and Departamento de Química Física, Universidad de Málaga, Campus de Teatinos s/n, 29071 Málaga, Spain

Received: July 29, 2005

The synthesis and a combined spectroscopic and density functional theoretical characterization of a 3′,4′-ethylenedioxy-5,5″-bis(dicyanomethylene)-5,5″-dihydro-2,2′:5′,2″-terthiophene analogue of 7,7,8,8-tetracyanoquinodimethane (TCNQ) are presented. Electrochemical data show that this novel trimer can be both reversibly reduced and oxidized at relatively low potentials. Quantum-chemical calculations show that the compound exhibits a quinoidal structure in its ground electronic state and that a certain degree of intramolecular charge transfer takes place from the central terthienyl moiety toward both $=C(CN)_2$ end-caps. Therefore, the amphoteric redox behavior of this novel material can be related to the coexistence of an electron-impoverished terthienyl core endowed by two electron-enriched $=C(CN)_2$ substituents. The UV−vis spectrum is dominated by the appearance of a strong absorption near 660 nm, attributable to the highest occupied molecular orbital (HOMO) → lowest unoccupied molecular orbital (LUMO) $\pi-\pi^*$ electronic transition of the terthienyl spine on the basis of time-dependent density functional theory (DFT) computations. The DFT calculations performed on the minimum-energy molecular geometry about the equilibrium atomic charge distribution, topologies, and energies of the frontier orbitals around the gap and about the Raman-active vibrations associated with the strongest Raman features are also consistent with a rather effective π-electron conjugation and the partial degree of intramolecular charge transfer mentioned above. Our study reveals this novel heteroquinoid trimer could act as a promising candidate in organic field-effect transistor (OFET) applications.

I. Introduction

Oligothiophenes have attracted considerable attention over the past few years for their use as the active component in many organic device technologies[4] including, but not limited to, organic field-effect transistors (OFETs) and complementary circuits.[1−4] Most oligothiophenes developed so far typically behave as hole transporters (p-type). However, environmentally stable electron-transporting (n-type) materials which could approach or even surpass the carrier mobilities of the most efficient p-type oligomeric (semi)conductors already available[3] are also required for the fabrication of p−n heterojunctions and complementary circuits. The operating characteristics of these organic-based electronic devices strongly depend on the charge-transport properties of the active component, which are indeed closely related to the energies of the highest occupied molecular orbital (HOMO) and lowest unoccupied molecular orbital (LUMO) frontier orbitals (governing the charge injection) and to the splitting of those levels in the solid state due to intermolecular interactions (determining the charge mobilities).[5] Thus, the extent of electronic coupling between HOMO levels controls the hole transport, whereas that between LUMO levels modulates the electron transport. Therefore, the understanding at the molecular scale of precise structure−property relationships plays a key role in the rational design of novel high-performance electron-transporting molecular materials.

Quinoidal oligothiophenes inherently display a smaller HOMO−LUMO energy gap than usual aromatic oligothiophenes, thus making ambipolar or dual (both p- and n-type) charge transport more likely because smaller gate voltages are required to populate the HOMO and LUMO levels (valence and conduction bands) with charge carriers.[6] Recently, a group at the University of Minnesota successfully achieved ambipolar transport in OFETs based on a quinoidal 3′,4′-dibutyl-5,5″-bis(dicyanomethylene)-5,5″-dihydro-2,2′:5′,2″-terthiophene taking advantage of a prior electrochemical analysis of this quinodimethane analogue which suggested its potential ability as n-channel semiconductor,[7] which is unusual for common oligothiophenes. To our knowledge, similar ambipolar transporters are rather scarce and even far less developed than p-type semiconductors.[8] In fact, the aforementioned **Bu_2T3CN4** heteroquinoid compound constitutes the first example of ambipolar transport in a thin-film transistor (TFT) based on a single semiconductor π-conjugated oligomer. The electron field-effect mobilities measured for the vapor- and solution-cast films of **Bu_2T3CN4** were 0.005 and 0.002 $cm^2/(V\ s)$, respectively.[7] These initial values were further improved up to 0.2 $cm^2/(V\ s)$,[7] close to the highest electron mobility of 0.6 $cm^2/(V\ s)$ reported so far for an organic TFT.[1e] These relatively high carrier mobilities are accounted for by the effectiveness of the

* Corresponding author. E-mail: teodomiro@uma.es.
† Istituto CNR di Scienze e Tecnologie Molecolari.
‡ E-mail: anna.berlin@istm.cnr.it.
§ Istituto CNR per L'Energetica e le Interfasi.
|| E-mail: g.zotti@ieni.cnr.it.
⊥ Universidad de Málaga.

10.1021/jp054204j CCC: $30.25
Published on Web 11/02/2005

intermolecular interactions, which determine the solid-state splitting of the HOMO and LUMO levels.[9]

Infrared and Raman spectroscopies provide useful information about molecular structures and intra- and/or intermolecular interactions. Vibrational analysis uses the normal modes of a molecule as microscopic probes of its structure. One could, therefore, assess valuable information on fundamental characteristics of this kind of amphoteric heteroquinoid systems from the analysis of their vibrational spectra as regarding, for example, the degree of electronic interaction between the different building blocks (i.e., dicyanomethylene end-caps, terthienyl core, and eventual side groups), the preferred molecular conformation, and the intermolecular interactions taking place in the solid state or solution. To evaluate all of this spectroscopic information, one first needs a theoretical model that allows a reliable relationship to be established between the vibrational spectra of the π-conjugated molecule and its electronic structure. We will make use throughout this manuscript of the nowadays widely accepted *effective conjugation coordinate* (ECC) theory proposed by G. Zerbi et al.[10] Second, the availability of numerous experimental/theoretical data from the previous analysis of the vibrational spectra of related molecules is also highly desirable for comparison purposes. Fortunately, vibrational data are at present available for a large number of aromatic and quinoid oligothiophenes.[11−13]

The outstanding charge-transport properties of **Bu_2T3CN4** demonstrate that quinoidal oligothiophenes constitute a new class of semiconductors with promising device applications.[7] Here, we report on the synthesis and characterization of a novel heteroquinoid 7,7,8,8-tetracyanoquinodimethane (TCNQ) analogue, 3′,4′-ethylenedioxy-5,5″-bis(dicyanomethylene)-5,5″-dihydro-2,2′:5′,2″-terthiophene (i.e., hereafter referred to as **TETCN4**) by means of spectroscopic techniques, electrochemistry, and density functional theory (DFT) quantum-chemical calculations. It is interesting to wonder in which aspects **TETCN4** differs from their unsubstituted and butyl substituted parents (**T3CN4** and **Bu_2T3CN4**, respectively) and to what extent the insertion of a ethylenedioxy group in the central ring could improve the conjugational properties assuming the benefits of electron release and rigidification through S···O interactions. This is the objective of the present paper, while the device performance of **TETCN4** is now under investigation.

II. Experimental and Computational Details

Chemicals and Reagents. All reactions of air- and water-sensitive materials were performed under nitrogen. The solvents used in the reactions (Fluka) were absolute and stored over molecular sieves. All other chemicals were reagent grade and used as received. 5,5″-Dibromo-3′,4′-ethylenedioxy-2,2′:5′,2″-terthiophene was prepared as described in the literature.[14]

5,5″-Bis(dicyanomethylene)-3′,4′-ethylenedioxy-5,5″-dihydro-2,2′:5′,2″-terthiophene (TETCN4). Malononitrile (85 mg, 1.29 mmol) was added to a suspension of sodium hydride (110 mg, 60% in oil, 2.75 mmol) in 1,2-dimethoxyethane (10 mL) at 0 °C. The reaction mixture was stirred for 30 min at room temperature, and then, 5,5″-dibromo-3′,4′-ethylenedioxy-2,2′:5′,2″-terthiophene (250 mg, 0.54 mmol) and $PdCl_2(PPh_3)_2$ (37 mg, 0.05 mmol) were added. The resulting mixture was heated under reflux for 4 h, then it was cooled to 0 °C, and then a saturated Br_2/H_2O solution (10 mL) was added. Water was added (5 mL), and the solid precipitated was collected by filtration under vacuum, washed with water, and dried. The product was purified by flash chromatography by sequentially eluting the column with CH_2Cl_2, 98/2 CH_2Cl_2/ethyl acetate, and 90/10 CH_2Cl_2/ethyl acetate to give the title compound as a dark solid (131 mg, 56% yield); mp > 300 °C. HREIMS: calcd, 431.9809; found, 431.9813. Anal. Calcd for $C_{20}H_8N_4O_2S_3$: C, 55.51; H, 1.85; N, 7.40. Found: C, 55,37; H, 1.96; N, 7.29.

UV−vis−NIR absorption spectra were recorded at room temperature either on a Lambda 19 Perkin-Elmer dispersive spectrophotometer or on an Agilent 8453 instrument equipped with a diode array for the fast recording of all of the absorptions appearing in the 190−1100 nm spectral region. FT-IR spectra were recorded on a Bruker Equinox 55 spectrometer. The compound was ground to a powder and pressed in a KBr pellet. FT-IR spectra, with a spectral resolution of 2 cm^{-1}, were collected over an average of 50 scans. Interference from atmospheric water vapor was minimized by purging the instrument with dry argon before starting the data collection. FT-Raman scattering spectra were collected on a Bruker FRA 106/S apparatus with a Nd:YAG laser source ($\lambda_{exc} = 1064$ nm) in a backscattering configuration. The operating power for the exciting laser radiation was kept at 100 mW in all of the experiments. Samples were analyzed as pure solids in sealed capillaries and dilute CH_2Cl_2 solutions (supplied by Aldrich with analytical grade). Typically, 1000 scans with 2 cm^{-1} spectral resolution were averaged to optimize the signal-to-noise ratio.

All electrochemical measurements were performed in dichloromethane of reagent grade (Uvasol, Merck) with a water content <0.01%. Tetrabutylammonium perchlorate of reagent grade was purchased from Fluka and used as the supporting electrolyte (0.1 M) as received. Cyclic voltammetry analysis was run in three electrode cells at 25 °C on solutions previously deaerated by N_2 bubbling and keeping a continuous nitrogen gas flow during the whole experiment. The counter electrode was platinum; the reference electrode was a silver/0.1 M silver perchlorate in acetonitrile (0.34 V vs SCE). The voltammetric apparatus (AMEL, Italy) included a 551 potentiostat modulated by a 568 programmable function generator and coupled to a 731 digital integrator. The working electrode for cyclic voltammetry was a platinum (0.003 cm^2) minidisk electrode.

DFT calculations were carried out using revision A.1 of the Gaussian 03 program package[15] running on an SGI Origin 2000 computer. Calculations of the optimized geometry, electronic excitation energies, and vibrational spectra were performed on a single molecule in a vacuum using Becke's three-parameter B3LYP exchange-correlation functional.[16] The 6-31G** basis set[17] was chosen as a compromise between accuracy and applicability to large molecules. Molecular orbital contours were plotted using Molekel 4.3.[18] Vertical excitation energies were computed for the 15 lowest energy electronic excited states by using the time-dependent DFT (TDDFT) approach.[19,20] This approach has been widely used to study the electronic spectra of large π-conjugated systems such as polyenes;[22] polycyclic aromatic hydrocarbons;[23,24] fullerenes;[25] oligomers of α-thiophenes, *p*-phenylenes, and *p*-phenylenevinylenes;[26] and porphyrin-type macrocycles and oligomers.[27,28] Standard hybrid functionals such as BLYP and B3LYP have been shown to provide excitation energies that are roughly within 0.3 eV of the experimental data. Despite these encouraging results, the TDDFT approach should be used with caution, since excitation energies can be affected by different errors. Overestimations/underestimations in the 0.4−0.7 eV range are not infrequent,[22,23e,f] and they can lead to misassignments when trying to provide a full interpretation of the electronic spectrum.[29]

The calculated harmonic vibrational frequencies were scaled down uniformly by a factor of 0.96, as recommended by Scott and Radom.[30] All of the theoretical vibrational data quoted in

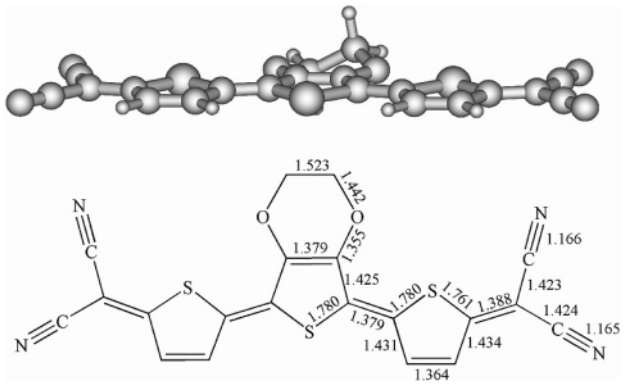

Figure 1. Lateral view of the optimized molecular structure of **TETCN4** and B3LYP/6-31G** values for selected skeletal bond lengths.

the text are thus scaled values. The theoretical infrared and Raman spectra were obtained by convoluting the scaled frequencies with Gaussian functions (10 cm^{-1} width at the half-height). The height of the Gaussians was determined from the IR intensities and Raman scattering activities calculated for the IR- and Raman-active normal modes, respectively. The IR intensities were calculated from the dipole moment derivatives with respect to normal coordinates, while polarizability derivatives for Raman activities were obtained using numerical differentiation of the analytical dipole moment derivatives with respect to the applied electric field.

III. Results and Discussion

Structure Calculations on the Neutral Compound. DFT//B3LYP/6-31G** model chemistry predicts a nearly planar structure for **TETCN4** with a transoid configuration of the sulfur atoms in adjacent rings and with the two methylene groups of the EDO chain pointing out at opposite sides of the π-conjugated backbone due to the sp^3 hybridization, thus leading to a C_2-type minimum-energy molecular structure. Regarding the main bond lengths calculated at the B3LYP/6-31G** level, the terthienyl moiety bears a quinoid structure in which the shortest carbon−carbon (CC) distances correspond to the $C_\beta-C_\beta$ bonds of the thiophene rings, to the inter-ring $C_\alpha-C_\alpha'$ bonds, and to the bonds connecting the oligothiophene spine to the dicyanomethylene end-caps (see Figure 1). Thus, the π-conjugated backbone of **TETCN4** exhibits a reversal of the single−double bond alternation pattern with respect to that usually found in aromatic α,α'-oligothiophenes, for which the $C_\beta-C_\beta$ bonds and the $C_\alpha-C_\alpha'$ bonds are longer than the $C_\alpha-C_\beta$ bonds.[31−33] In fact, the quinoid structure of **TETCN4** shows a great resemblance to those theoretically predicted for the dicationic species of common aromatic oligothiophenes.[34]

The mean single−double CC bond-length alternation pattern (BLA) parameters for the outer and inner thiophene rings amount to −0.069 and −0.046 Å, respectively, which is indicative of an increasing degree of quinoidization from the central ring toward both ends of the quinoidal trimer. Scheme 1 displays a set of simple resonant forms describing the mesomeric electron releasing effect of the EDO side group and the comparison with the role of the thienyl chain. It is deduced that the electronic coupling of the lone electron pairs of the oxygens through the thienyl chain might enhance the aromaticity of the central ring, with the total effect being a bond-length equalization (BLA closes to zero) of these three innermost CC bonds. This theoretical finding is in contrast with the more marked quinoidal character of the outermost thienyl rings likely

SCHEME 1: Limit Resonant Forms Describing the Interactions of the EDO Group and the Thienyl Chain with the Dicyanomethylene Groups and B3LYP/6-31G Optimized Geometries of TETCN4 and T3CN4**

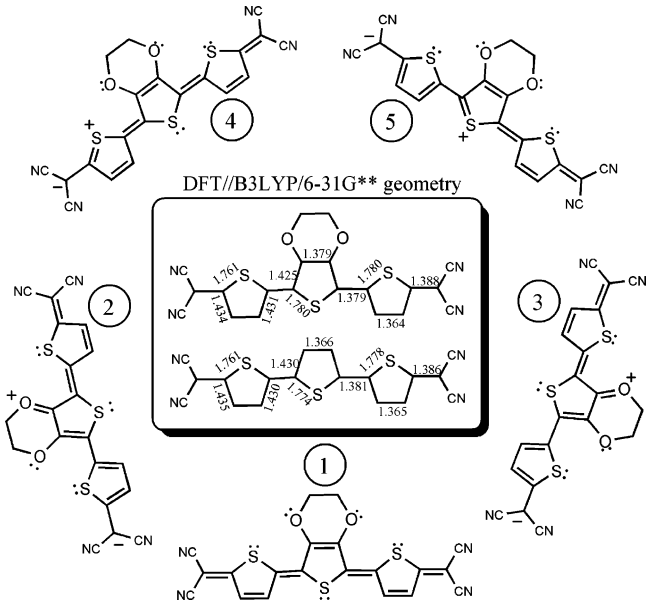

due to the proximity of the very strong electron-withdrawing dicyanomethylene groups. In the case of the quinoidal 5,5″-bis(dicyanomethylene)-5,5″-dihydro-2,2′:5′,2″-terthiophene, however (i.e., the homogeneous terthienyl counterpart of **TETCN4**, which can be termed as **T3CN4**), the computed BLA values at the B3LYP/6-31G** level result in being almost identical for both the inner (−0.066 Å) and outer (−0.068 Å) rings, stressing the electronic and structural intervention of the EDO group as described above.[11] In **Bu_2T3CN4**, the BLAs for the inner and outer thienyl rings are respectively −0.054 and −0.069 Å, revealing an intermediate actuation of these butyl chains in the central ring regarding the effects of EDO substitution and unsubstitution.[11] These facts agree with a $C(sp^3) \rightarrow C(sp^2)$ σ-inductive electron release for **Bu_2T3CN4** in contrast with an $O(sp^2) \rightarrow C(sp^2)$ π-resonant interaction for **TETCN4**.

It is quite instructive to discuss some additional structural data related to the balancing role played by the EDO and the terthienyl chain regarding dicyano encapsulation, such as it is rigidly sketched by the resonant structures in Scheme 1. (i) The main B3LYP/6-31G** structural features for the thienyl chain are stated by its quinoidization through coupling the two $(CN)_2$ groups (resonant form 1). However, particular properties of this quinoidal structure are dictated by the interaction of the EDO functionalization and, to a lesser extent, by the sulfurs. (ii) As shown above, the quinoidization imposed by the electron-withdrawing external groups is mitigated in the central ring bearing the electron releasing EDO group, a phenomenon outlined by resonant forms 2 and 3. (iii) The asymmetry of the C−S bonds in the external thienyl rings is accounted for by the role played by resonant form 4. (iv) Analogously, the intervention of the innermost sulfur atom (resonant form 5) in the description of the actual B3LYP/6-31G** geometry is rather negligible as accounted for by their large C−S bonds (1.780 Å) in comparison with those of the external rings (1.761 and 1.780 Å for the affected and unaffected bonds). Even more interesting, these B3LYP/6-31G** C−S bond distances in **T3CN4** are 1.774 Å, revealing the vanishing of the inner S

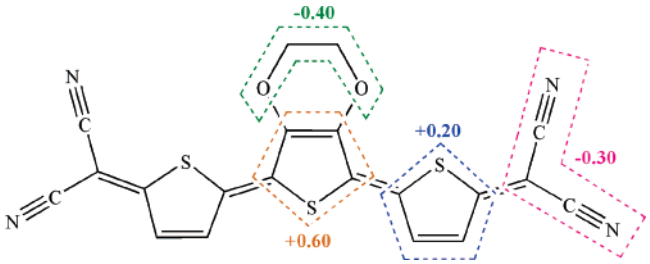

Figure 2. Atomic overall charges on various molecular domains of **TETCN4** as derived from the Mulliken population analysis at the DFT// B3LYP/6-31G** level of theory.

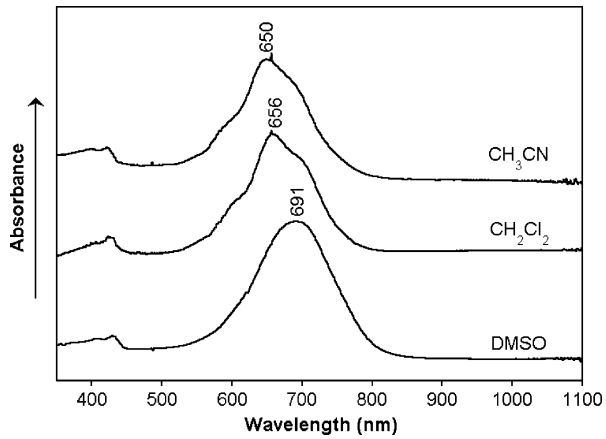

Figure 3. UV−vis−NIR absorption spectra of **TETCN4** in CH_2Cl_2, CH_3CN, and DMSO solutions.

coupling with the external $(CN)_2$ in **TETCN4** likely due to the cross-conjugated interference as stated by resonant forms 2, 3, and 5.

The B3LYP/6-31G** net atomic charges calculated using Mulliken population analysis indicate that each dicyanomethylene group supports a negative charge of −0.30*e*, which is balanced by the outer rings (+0.20*e*), the central ring (+0.60*e*), and the ethylenedioxide chain (−0.40*e*) (see Figure 2). This drift of the electron density from the central spine of the quinoidal trimer toward both electron-withdrawing $=C(CN)_2$ groups can be outlined by the resonant forms as well. The distribution of the electron charge can be viewed as the EDO and the sulfur atoms acting like an electron donor toward the electron-deficient C=C/C−C conjugated path which mediates the electron drift to the dicyanomethylene groups. The following two facts are significant in this analysis: (i) The amount of negative charge over the external $(CN)_2$ is slightly higher in **TETCN4** (−0.30*e*) than in **Bu$_2$T3CN4** (−0.29*e*) or in **T3CN4** (−0.28*e*), accounting for the additional charge release of the EDO groups. (ii) The charge borne by the central ring increases as +0.14*e* in **T3CN4**, +0.20*e* in **Bu$_2$T3CN4**, and +0.22*e* in **TETCN4**, while the opposite trend is predicted for the outermost rings upon going from **T3CN4** (+0.21*e*) to **TETCN4** (+0.20*e*). The inclusion of the EDO groups enhances the electron donation of the central moiety; however, its effect is not added directly to the overall charge transference but the release of electron density of the outer rings is mitigated. A possible explanation for this finding is the interference of all of the resonant forms in the C=C/C−C path giving rise to a partial coalescence of the S donation by the EDO → $C(CN)_2$ coupling.

Electronic Absorption Spectra. Figure 3 shows the UV−vis−NIR spectra recorded for **TETCN4** in CH_2Cl_2, CH_3CN, and DMSO solutions. The three spectra exhibit a strong, broad, and structured absorption extending from 550 to 800 nm with a maximum at ≈660 nm (1.88 eV). The wavelength of this absorption maximum is largely red-shifted with respect to the $\pi-\pi^*$ electronic transition aromatic oligothiophenes usually display in the visible region at ≈350−450 nm. In this regard, the $\pi-\pi^*$ absorption of unsubstituted α-linked terthiophene is found to occur at 355 nm (3.49 eV), whereas it is measured at 432 nm (2.87 eV) for the sexithiophene.[35] The shift to significantly longer wavelengths (namely, by nearly 300 nm) of the $\pi-\pi^*$ absorption band of **TETCN4** must be thus ascribed not solely to the extension of the π-conjugated path upon the attachment of the $=C(CN)_2$ end-caps but mainly to the evolution from an aromatic-like to a quinoid-like molecular structure.

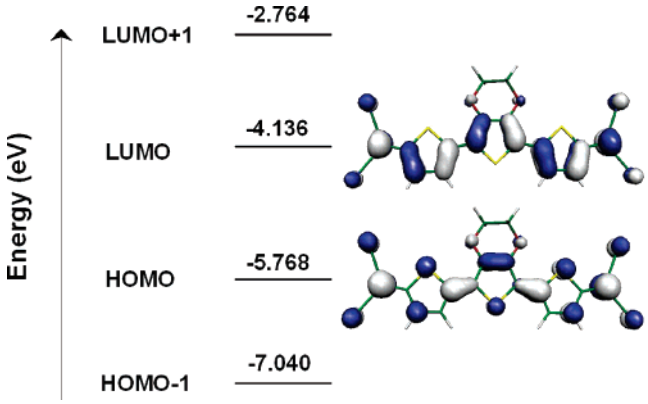

Figure 4. B3LYP/6-31G** electronic density contours (0.03*e*/bohr^3) for the frontier molecular orbitals of **TETCN4** and one-electron energies (ϵ_i) diagram around the band gap.

To gain a deeper insight into the optical properties of **TETCN4**, we decided to perform calculations of vertical one-electron excitation energies (i.e., by considering at least the 15 lowest energy electronic excited states) by means of the time-dependent DFT formalism and starting from the previously optimized ground-state B3LYP/6-31G** molecular geometry. Theoretical calculations predict the appearance of only one strong transition below 3.0 eV, corresponding to the excitation to the first excited singlet electronic state (S_1) and arising from the promotion of one electron from the highest occupied molecular orbital (HOMO) to the lowest unoccupied molecular orbital (LUMO). The strong absorption at ≈660 nm is therefore to be assigned, on the basis of the TDDFT// B3LYP/6-31G** theoretical data, to the $S_0 \rightarrow S_1$ electronic transition.

Figure 4 shows the atomic orbital compositions of the HOMO and LUMO of **TETCN4**. As expected, these two orbitals are of π-nature and spread over the whole conjugated path with large contributions by part of the $=C(CN)_2$ end-caps. The topologies of the HOMO and the LUMO are found to be clearly reversed with respect to those commonly computed for aromatic oligothiophenes[36] as a result of the quinoid structure of **TETCN4**. This topology-MO reversal determines that the HOMO−LUMO gaps of ≈1.63 eV (see Figure 4), computed at the B3LYP/6-31G** level both for **TETCN4** and for **T3CN4**, result in being much lower than that obtained for aromatic α-linked terthiophene (3.45 eV) at the same level of theory.[36] It is remarkable that both trimers present the same wavelength for their absorptions despite the fact that they intrinsically have different configurations. This effect probably has its origin in the participation, to a similar extent, of the oxygen atomic orbitals in the two HOMO and LUMO frontier orbitals, resulting in the energies of both terms actually being pushed up by +0.259 eV (HOMO) and +0.267 eV (LUMO) regarding **T3CN4** but the difference remains essentially unchanged. This prediction will also be confirmed with the modulation of the redox potentials upon EDO insertion in the following section.

The rather low energy of the $\pi-\pi^*$ absorption in the visible region is therefore intrinsically related to the heteroquinoid structure of both trimers. In addition, the topologies of the HOMO and LUMO show that the band experimentally measured at 660 nm originates in the $\pi-\pi^*$ transition of the central terthienyl spine and that no significant intramolecular charge transfer (ICT) toward the dicyanomethylene groups takes place, since both $=C(CN)_2$ end-caps equally participate in the two frontier molecular orbitals involved in such an electronic transition. The applicability of the TDDFT approach to donor−acceptor systems has been questioned in the literature, because it sometimes leads to large deviations for the excitation energies of charge transfer states.[37] However, this is not always the case,[38] and particularly, it does not affect the assignment of the $\pi-\pi^*$ transition of **TETCN4**, since this one-electron excitation does not involve a significant degree of ICT.

It is rather usual that the computed TDDFT energy for a vertical one-electronic transition from a doubly occupied MO to a vacant MO is predicted to be smaller than their energy gap, which can be accounted for in terms of the reduced interelectronic interaction upon the single electron excitation (i.e., the interaction can be conceptually interpreted in a simple way as the balance between Coulomb and exchange terms, and expectedly, it should progressively decrease with increasing molecular size of the π-conjugated system). This is not however the case for the **TETCN4** quinoidal trimer, for which the B3LYP/6-31G** HOMO−LUMO energy gap of 1.63 eV is found to be lower by 0.36 eV than the B3LYP/6-31G** energy predicted by the TDDFT approach for the only strong UV−vis−NIR absorption which should occur below 3.0 eV (i.e., at 1.99 eV, and with an oscillator strength, *f*, of 1.84). One of the reasons for this apparent discrepancy is that various vertical one-electron excitations apart from the HOMO → LUMO transition enter into play in the lowest-energy absorption band of the compound around 660 nm (i.e., the usually termed $\pi-\pi^*$ absorption peak has for these heteroquinoid systems a multiconfigurational character, although the largest contribution comes from the HOMO → LUMO excitation).

This fact must be stressed. First, despite being very often considered as a direct measure of the extent of π-conjugation in a system, UV−vis−NIR spectroscopic absorption data are not unambiguous for this purpose. One must be cautious when analyzing a homologous set of linear π-conjugated oligomers. It is not infrequent that the optical properties reach saturation for already quite short chain lengths, whereas the theoretical MO energies still continue to vary for longer oligomers. For such linear systems, the Coulomb and exchange integrals should decrease with increasing number of repeating units in the chain (this trend of variation is in agreement with the expectation that as the oligomer grows longer the interelectronic repulsion for a given doubly occupied MO should progressively decrease, particularly if such a MO spreads over the entire π-conjugated backbone). Nonetheless, it is usually found that, for a homologous set of oligomers, the narrowing of the HOMO−LUMO gap with increasing number of units in the π-conjugated chain is more pronounced, so that the Coulomb and exchange terms play a secondary role in determining the energy of the singlet excited state associated with the HOMO → LUMO transition (i.e., the situation could however be more complex and troublesome when studying, for example, the chain-length dependence of the optical properties of a bunch of mixed donor−acceptor alternating π-conjugated systems). As a result, it is desirable that the analysis of the experimental UV−vis−NIR data is not only based on the spectroscopic intuition but guided by some sort of quantum-chemical calculation about the topologies and energies of the MOs involved and of the multiconfigurational character of the different UV−vis−NIR absorptions.

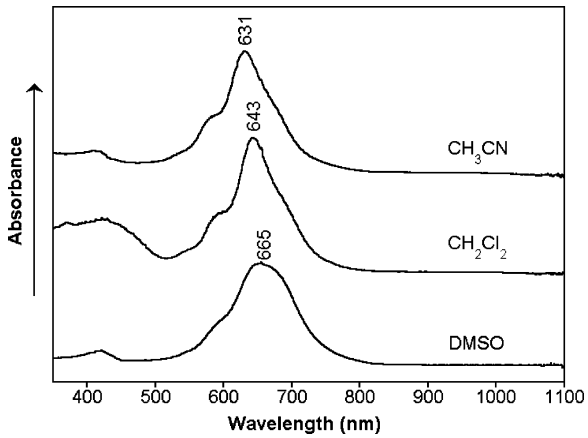

Figure 5. UV−vis−NIR absorption spectra of **T3CN4** in CH_2Cl_2, CH_3CN, and DMSO solutions.

Consideration of the details shows that the $\pi-\pi^*$ electromagnetic absorption of **TETCN4** in CH_2Cl_2 shows its maximum at 656 nm (1.88 eV) in addition to two other shoulders at both the lower and higher energy sides. These shoulders must be ascribed to vibronic components given the rigid heteroquinoid structure of the chromophore and since no electronic transitions other than the HOMO → LUMO are expected to occur below 3 eV on the basis of the TDDFT//B3LYP/6-31G** calculations. Vibronic structure has also been observed for the $S_0 \rightarrow S_1$ excitation of aromatic oligothiophenes.[39] The $\pi-\pi^*$ absorption of **TETCN4** displays a similar structured pattern in CH_2Cl_2 and CH_3CN solutions, but the various components are slightly red-shifted in the former medium. In passing to a more polar solvent like DMSO, the maximum of the $\pi-\pi^*$ absorption still experiences a further red shift by ≈30 nm, being now measured at 691 nm. Furthermore, as for the aforementioned **T3CN4** quinoidal trimer, the $\pi-\pi^*$ absorption is found to display a great resemblance with respect to that of **TETCN4**, although the maxima are slightly blue-shifted in the case of the former chromophore for all of the solvents studied: 631 vs 650 nm in CH_3CN, 643 vs 656 nm in CH_2Cl_2, and 665 vs 691 nm in DMSO (see Figure 5). It seems the EDO substitution of the central thiophene ring gives rise to a bathochromic shift of the $\pi-\pi^*$ absorption in any solvent, which becomes more pronounced with increasing polarity. Such a red shift was not noticed however upon the attachment of alkyl side chains to the β-positions of **T3CN4** and a series of thiophene-based quinodimethane dimers, for which the β-hexyl substitution in different regioregular configurations (i.e., H−H, H−T and T−T) affects only the maximum $\pi-\pi^*$ absorption wavelength by rather a few nanometers.[40] It is reasonably expected that **TETCN4** would display a favored disposition to charge separation (Scheme 1) due to the occurrence of specific interactions promoted by the EDO groups, and in this regard, more polar solvents would have a bigger impact on the stabilization of the ground/excited electronic states and therefore on the solvatochromic behavior.

Figure 6 shows the absorbance spectra of solvent-cast films of **TETCN4** and **T3CN4**. For both compounds, there is a shift of the highest and lowest energy edges of the $\pi-\pi^*$ absorption from ≈550 and 800 nm in dilute solution to wavelengths shorter and longer than 460 and 1000 nm, respectively, in the solid state (i.e., a broadening of the visible absorption due to the

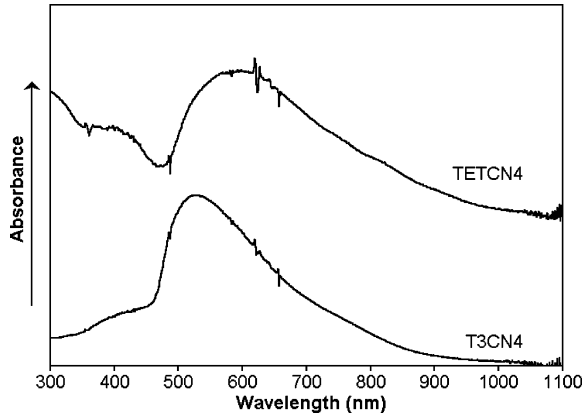

Figure 6. UV−vis−NIR spectra **TETCN4** and **T3CN4** as solvent-cast solid films.

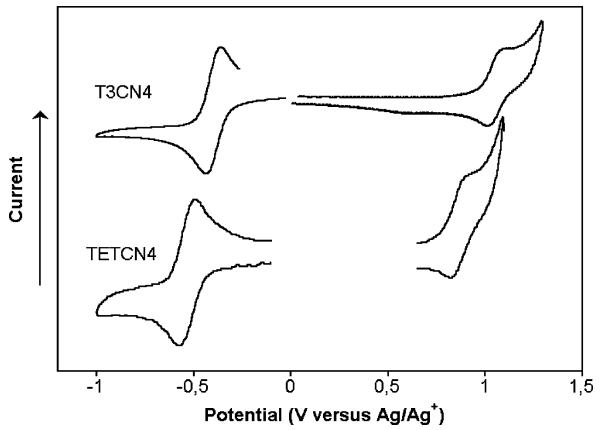

Figure 7. Cyclic voltammograms of **TETCN4** and **T3CN4** in 0.1 M Bu_4NClO_4/CH_2Cl_2 solution. The scan rate was 100 mV s^{-1}, and the reference electrode was Ag/0.1 M $AgClO_4$ in CH_3CN (0.34 V vs SCE).

HOMO → LUMO transition). In addition, the fine structure evidenced for both chromophores in dilute solution is completely absent in the films, whereas the value of λ_{max} seemingly upshifts to ≈530 nm in the solvent-cast film of **T3CN4** and to ≈590 nm in the case of **TETCN4**. These experimental observations may indicate that unresolved transitions are present in the solid-state UV−vis−NIR absorption spectra.

TETCN4 and other oligothienoquinoids[6g−i,7,11b,c] can be viewed as structural and electronic models of charge carriers in oxidized oligothiophenes. P-doping of aromatic oligothiophenes leads to the generation of various types of quinoid-like charged defects successively extending from the middle part of the oligomeric chain toward its ends (i.e., radical cations, dications, radical trications, and so on). In this regard, the heteroquinoid structure of the dications or positive bipolaron species has been spectroscopically demonstrated to extend over the whole π-conjugated path for relatively short oligomers such as end-capped α,α'-quaterthiophenes and sexithiophenes.[13] The UV−vis−NIR spectral fingerprint of these dications is a strong absorption at lower energies than the $\pi-\pi^*$ transition of the neutral oligomer (i.e., at ≈750−800 nm in quaterthiophenes and ≈950−1100 nm in sexithiophenes)[13,39a,41] which can be qualitatively correlated with the strong $\pi-\pi^*$ absorption of **TETCN4** at ≈660 nm.

Electrochemical Properties. Figure 7 displays the cyclic voltammograms recorded for **TETCN4** and **T3CN4** in CH_2Cl_2 solution. The **TETCN4** trimer exhibits a reversible two-electron reduction wave at $E^\circ_{red} = -0.53$ V (in fact two close one-electron processes at $E^\circ_{red} = -0.49$ and -0.57 V) and a reversible one-electron oxidation wave at $E^\circ_{ox} = 0.85$ V. There is a negative shift of both reduction and oxidation potentials as compared to **T3CN4** (particularly, for the oxidation). This effect is in agreement with that already announced in the previous section dealing with the affectation of the frontier molecular orbitals which, eventually, does not produce any change of the UV−vis−NIR absorption maxima of **TETCN4** and **T3CN4**. In a simple way, oxidations and reductions can be visualized as the extraction/incorporation of electrons of/in the HOMO/LUMO orbitals and, according to Koopman's theorem, a good approach between HOMO/LUMO energies and oxidation/reduction potential can be established. As discussed before, the EDO electron release destabilizes both HOMO/LUMO energies regarding those in **T3CN4** which justifies the cathodic shifts of both processes. The greater displacement of oxidation can be explained taking into account the larger stability of the generated cations, in contrast with the case of anions in reduction, due to the presence of electron-rich EDO groups. As will be outlined in the next paragraph, the greater electron releasing effect of EDO as compared with that of alkyl saturated chains will also impact the electrochemical properties.

TABLE 1: Redox Potentials for Some Quinoidal Oligothiophenes

monomer	E°_{ox}/V	E°_{red}/V
TETCN4	0.85	−0.49; −0.57
T3CN4	1.05	−0.37; −0.43
H3T3CN4[a]	0.98	−0.40
H4T4CN4[a]	0.58; 1.12	−0.31
T2CN4	1.55	−0.37; −0.60

[a] From ref 6i.

The redox potentials of **TETCN4** and **T3CN4** can be compared with those previously measured by us for two other regioregular heteroquinoid TCNQ analogues having three and four α-linked thienyl units (i.e., each of them bearing β-hexyl chains), hereafter termed as **H3T3CN4** and **H4T4CN4** (see Table 1).[6i] Both oligomers exhibited a reversible two-electron reduction wave at $E^\circ_{red} = -0.40$ and -0.31 V, respectively. This wave corresponds to the reduction of both dicyanomethylene groups and leads to the generation of a dianion. The less negative E°_{red} value of the tetramer compared to that of the trimer is a consequence of the mitigation of the on-site Coulomb repulsions between the two injected charges as the oligomer grows longer. By comparing the electrochemical data of the three trimers, we see that the attachment of an EDO chain on the central thienyl unit has a larger effect on the redox potential values than the substitution of each thienyl unit by a hexyl group. Previous electrochemical studies for a set of **T2CN4**-type dimers indicated two sequential one-electron reductions, as also evidenced for TCNQ.[6g,h] The difference of nearly 0.2 V between the two reduction potentials recorded for these bithienoquinoid derivatives was however significantly smaller than that measured for TCNQ (0.72 V), suggesting a decrease of the on-site Coulomb repulsion in the dianionic state of the former compounds. As expected, the Coulomb repulsion is even smaller for the longer oligomers (i.e., 0.08 V in the case of **TETCN4**), and the observation of a single two-electron reduction process indicates that the anion radical is less stable than the dianion or at least of comparable stability so that the two processes occur under the same reduction wave.

In view of their chemical structures, these heteroquinoid TCNQ analogues are expected to be electron deficient due to the electron-withdrawing dicyanomethylene groups, and oxidation potentials higher than those measured for the corresponding aromatic oligothiophenes might be anticipated. As aforementioned, **TETCN4** displays a reversible one-electron oxidation

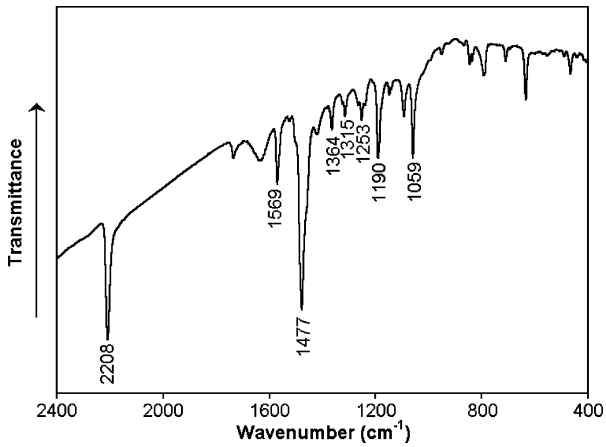

Figure 8. Fourier transform infrared spectrum of **TETCN4** in the form of a KBr pellet over probe energies of 2300−400 cm^{-1}.

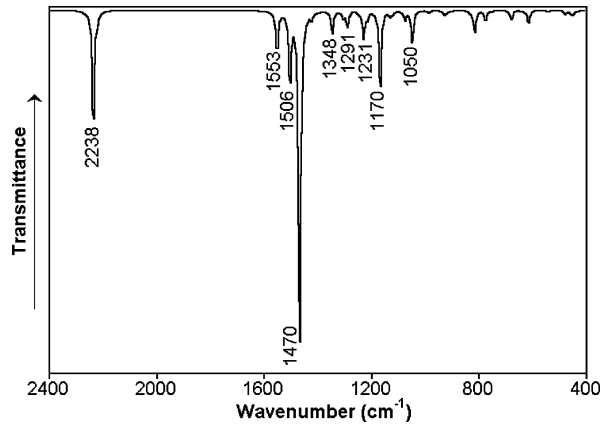

Figure 9. Theoretically calculated (B3LYP/6-31G**) IR spectrum of **TETCN4**.

process at $E°_{ox}$ = 0.85 V versus Ag/Ag^+ (1.2 V vs SCE); the generation of the radical cation thus takes place at a voltage intermediate between those of bithiophene and terthiophene.[42] The occurrence of reversible oxidation and reduction processes on a given oligothienyl chain may have important implications in new technologies and reveals the ability of these molecular materials to act both as electron donors and as electron acceptors in a wide range of potential values.

Infrared and Raman Spectroscopic Results. The FT-IR spectrum of **TETCN4** in the solid state is shown in Figure 8, whereas Figure 9 depicts the computed one at the B3LYP/6-31G** level. The theoretical data nicely reproduce the shapes, relative intensities, and peak positions of the experimental features in the whole spectral range between 2300 and 400 cm^{-1}. A continuous rising of the background absorption is observed toward the higher frequency side of the experimental FT-IR spectrum. This is due to the scattering produced by the sample and the overlap of the vibrational spectrum over the tail of the solid-state $\pi-\pi^*$ transition in the NIR region.

The C≡N stretching vibration is measured as a sharp and strong absorption at 2208 cm^{-1}. The shift toward lower frequencies of this vibration upon complexation of TCNQ with electron donors has been related in the past to the degree of charge transfer in organic conducting salts, since its peak position is highly sensitive to the electron density borne by the electron-deficient CN bonds.[43] The ν(CN) IR absorption also significantly red shifts upon reduction of these heteroquinoid compounds. For instance, the CN stretching is measured at 2225 cm^{-1} for neutral TCNQ, at 2197 cm^{-1} for $TCNQ^-$, and at 2164 cm^{-1} for $TCNQ^{2-}$.[44,45] Using these data to correlate the ν(C≡N) frequency and the net charge per $=C(CN)_2$ group, the electron density transferred from the central TET spine to each dicyanomethylene end-cap is estimated to amount to 0.26*e*, in good accordance with the theoretical B3LYP/6-31G** value 0.29*e*. On the other hand, the slight downshift by 2 cm^{-1} of the ν(CN) infrared band upon going from **TETCN4** to **T3CN4** and **Bu2T3CN4** (2210 cm^{-1}) corroborates experimentally the comparative analysis about the modulation of the electron density drift or polarization toward the electron-withdrawing groups from the central thienyl spine.

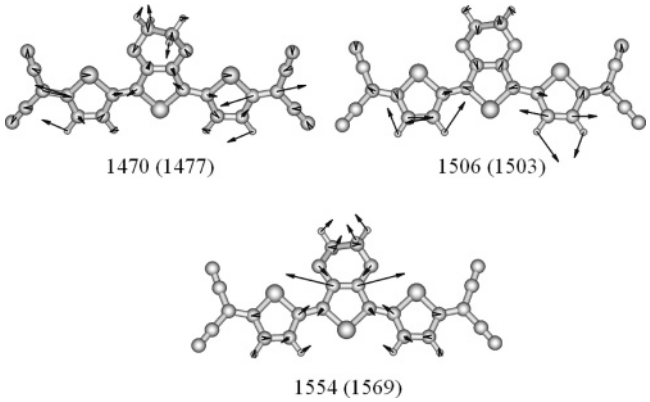

Figure 10. B3LYP/6-31G** eigenvectors for selected IR-active absorptions of **TETCN4**. Scaled and experimental (in parentheses) wavenumbers are given in inverted centimeters.

The infrared spectrum over the 1600−1000 cm^{-1} frequency range provides useful structural information about the π-conjugated backbone. The strongest IR absorption at 1477 cm^{-1} and the medium-weak bands at 1503 and 1569 cm^{-1} are assigned to the normal modes calculated at 1470, 1506, and 1554 cm^{-1}, respectively. As sketched in Figure 10, these three modes describe antisymmetric stretching vibrations of the C=C bonds: (i) The mode at 1554 cm^{-1} implies a large displacement of the $C_\beta=C_\beta$ bond of the EDOT unit from its equilibrium position, being also coupled to some extent with the stretches of the inter-ring $C_\alpha=C_\alpha'$ bonds. (ii) That at 1506 cm^{-1} originates in the out-of-phase motion of the $C_\beta=C_\beta$ bonds of the two thienyl rings, coupled with the stretchings of the $C_\alpha=C_{sp2}$ bonds connecting the outermost rings to the $C(CN)_2$ end-caps. (iii) However, the strongest IR-active mode at 1470 cm^{-1} involves a collective vibration of the π-conjugated backbone along which the inter-ring $C_\alpha=C_\alpha'$ and $C_\alpha=C(CN)_2$ double bonds linked to one of the thienyl rings vibrate in *opposite phase* with respect to their symmetry counterparts in the other half-molecule. The latter two IR-active modes are recorded at 1528 and 1499 cm^{-1}, respectively, for the **T2CN4** dimer, for which they also give rise to the strongest IR features below 1600 cm^{-1}.[11c] The lower frequency values measured here for **TETCN4** as compared with **T2CN4** are due to the combined effects of the attachment of an electron-donating EDO side chain to the central ring and the extension of the π-conjugated C=C/C−C path.

The band at 1364 cm^{-1} (calculated at 1348 cm^{-1}) is due to the antisymmetric stretching of the $C_\alpha-C_\beta$ bonds sizeably mixed with in-plane thienyl $\delta(C_\beta-H)$ bendings and aliphatic $\delta(CH_2)$ deformations of the EDO side chain (see Supporting Information Figure S1). The absorption recorded at 1315 cm^{-1} (predicted at 1291 cm^{-1}) is due to a similar mode but with a higher contribution by part of the $C_\alpha-C_\beta$ bonds of the central EDOT moiety. The sets of medium-weak IR absorptions between that at 1253 cm^{-1} (calculated at 1231 cm^{-1}) and that at 1059 cm^{-1} (computed at 1050 cm^{-1}) can also be described as different skeletal stretching vibrations of the $C_\alpha-C_\beta$ bonds with large

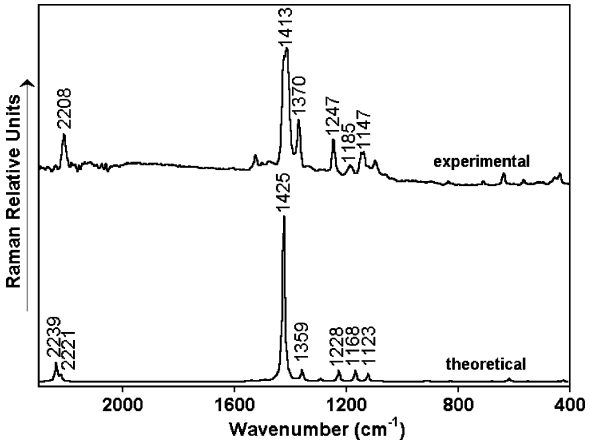

Figure 11. Comparison between the FT-Raman spectrum of **TETCN4** recorded on the pure solid sample over probe energies of 2300−400 cm^{-1} (a) and the theoretical one computed at the B3LYP/6-31G** level (b).

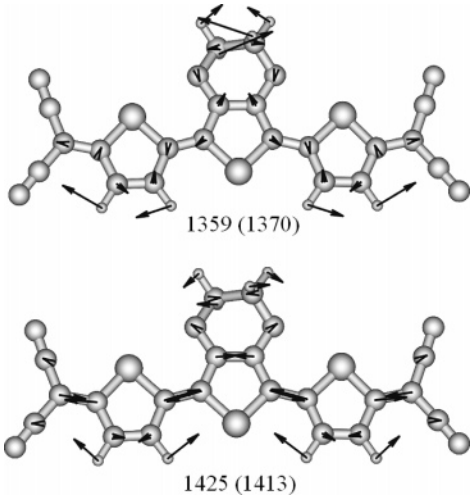

Figure 12. B3LYP/6-31G** eigenvectors associated with selected Raman-active vibrations of **TETCN4**. Scaled and experimental (in parentheses) wavenumbers are given in inverted centimeters.

contributions from the stretches of the C_{sp2}—C "*single bonds*" of the $=C(CN)_2$ end-caps and in-plane thienyl $\delta(C_\beta—H)$ and aliphatic $\delta(CH_2)$ bendings. A representative eigenvector for these IR absorptions is that shown in Supporting Information Figure S1 for the normal mode calculated at 1170 cm^{-1}, which gives rise to the most outstanding peak in this region at 1190 cm^{-1}.

Finally, whereas, for aromatic oligothiophenes, the out-of-plane γ(C−H) deformations are usually found to give rise to the strongest by far IR absorptions near 780−795 cm^{-1},[11a] they display a rather weak IR activity for this class of heteroquinoid compounds.

The Fourier transform Raman scattering profile collected for solid **TETCN4** in the 2400−400 cm^{-1} energy region is displayed in Figure 11 together with the theoretical B3LYP/6-31G** one (Figure 12 sketches the eigenvectors associated with the main features).

In the experimental spectrum, the ν(C≡N) vibration appears as a strong scattering at 2208 cm^{-1}. Theoretically, two different normal modes at 2239 and 2221 cm^{-1} are found to contribute to this Raman band. The former corresponds to an antisymmetric vibration in which the two CN bonds of each $=C(CN)_2$ group vibrate in phase, whereas the latter is due to a symmetric mode in which the CN bonds of each $=C(CN)_2$ end-cap vibrate out of phase.

The experimental Raman profile in the 1600−400 cm^{-1} region is somewhat simpler than the FT-IR (despite the absence of molecular symmetry due to the tilting of the ethylenedioxy chain out of the least-squares plane defined by the thienyl units). This is a common finding in most π-conjugated linear systems. The unusual vibrational spectra of π-conjugated molecules are fully rationalized within the framework of the *effective conjugation coordinate* (ECC) theory.[10] This theory states the existence of a collective vibrational mode, the ECC mode, which consists of a linear combination of ring C=C/C—C stretching vibrations. The associated frequency is an average of the strengths of the double and single bonds of the conjugated units. In aromatic oligothiophenes, electronic interactions between adjacent thiophene rings give rise to the delocalization of the π-electrons.[46] The structural relaxation upon chain elongation results in a slight lengthening of the $C_\alpha=C_\beta$ bonds and in a shortening of the $C_\alpha—C_\alpha'$ and $C_\beta—C_\beta$ bonds, along the conjugation pathway. For oxidized oligothiophenes, the $C_\alpha=C_\beta$ bonds of the originally aromatic structure lengthen, while the $C_\alpha—C_\alpha'$ and $C_\beta—C_\beta$ bonds shorten, as oxidation takes place. The molecular structure evolves into a progressively more quinoid-type geometry. Therefore, the frequency of the ECC mode (mainly made up of C=C stretching vibrations) downshifts with an increase in either the length of the π-conjugated oligomer or the quinoid character of the oligothiophene backbone.[11−13]

The characteristic ECC mode is usually found to originate the strongest Raman feature of the spectrum. Its associated eigenvector describes the evolution of the π-conjugated backbone from an aromatic-like pattern (HOMO orbital) to a quinoide-like pattern (LUMO orbital) in aromatic oligothiophenes and the opposite trend for quinoidal oligothiophenes. This means that the collective ECC mode involves the easiest (least energetic) way to move many atoms while, at the same time, inducing large changes of the electron density. This gives rise to the largest variation of the molecular polarizability and, consequently, to the strongest intensity for the ECC mode among all of the Raman-active vibrations. The physical mechanism that sets up this phenomenon is known as the electron−phonon coupling mechanism.[47]

The Raman bands at 1413 and 1370 cm^{-1} are the strongest features of the spectrum and are calculated at 1425 and 1359 cm^{-1}, respectively. As sketched in Figure 12, the eigenvector for the 1425 cm^{-1} mode corresponds to a totally symmetric ν(C=C)/ν(C—C) collective stretching spreading over the whole terthienoquinoid spine, along which all double C=C bonds lengthen in phase while all single C—C bonds shrink in phase. This normal mode describes the evolution from a heteroquinoid structure to a heteroaromatic configuration of the π-conjugated skeleton and, therefore, corresponds to the ECC mode. On the other hand, the band calculated at 1359 cm^{-1} arises from a $\nu(C_\alpha—C_\beta)$ stretching vibration, coupled with inter-ring $\nu(C_\alpha=C_\alpha')$ motions and in-plane thienyl $\delta(C_\beta—H)$ bendings (see Figure 12).

As for the **T3CN4** trimer, the ECC mode was assigned to the strongest Raman scattering at 1428 cm^{-1}.[11b] The 15 cm^{-1} downshift followed by the ECC mode in going from **T3CN4** to **TETCN4** is a new validation of our hypothesis dealing with the important effect of the EDO group in the conjugational properties of **TETCN4** relative to **T3CN4** or others. The existence of a new conjugated channel accounting for the electron releasing effect of the oxygens toward the thienyl chain, which provokes a larger degree of bond equalization in the central ring of **TETCN4** than in **T3CN4**, is at the origin of the structural relaxation and shift of the ECC modes from one to

another. The comparison with the Raman spectrum of **Bu_2T3CN4** is more complex due to the mechanical coupling of the ν(C═C/C—C) vibrations with the $\beta(CH_2)/\beta(CH_3)$ modes of the side chain which downshifts up to 1382 cm^{-1} the ECC mode in this quinoid. It must be mentioned that Raman wavenumbers (no so intensities) are observable quantities related to the structure of the ground electronic state and therefore they outline a new way to get insight of the affectation of the quinoidal structure upon β-substitution. Very recently, we have shown that the position of the Raman ECC mode is directly controlled by the electronic effects between (±) inductive and mesomeric groups toward the oligothienyl chain. The reader is referred to this work to have a deep understanding of the electronic interactions monitored by Raman spectroscopy in this class of conjugated systems.[48]

The medium Raman scattering recorded at 1247 cm^{-1} is due to the normal mode computed at 1228 cm^{-1}, which describes a totally symmetric skeletal ν(CC) stretching with all of the C_α—C_β thienyl bonds vibrating in phase and strongly coupled to the stretches of the C_{sp2}—C *single bonds* of the ═$C(CN)_2$ end-caps (see Supporting Information Figure S2). The bands at 1185 and 1147 cm^{-1} can be easily correlated with the theoretical modes at 1168 and 1123 cm^{-1}, and they are also due to totally symmetric $\nu(C_\alpha—C_\beta)$ stretchings of the various thienyl units but are now more extensively coupled to in-plane $\delta(C_\beta—H)$ bendings and less to the ν(C—C) stretches of the end-caps. Finally, Raman bands below 1000 cm^{-1} are not very interesting from the structural point of view because they are not directly related to the π-electron conjugation pathway. This determines that all of these Raman lines are not selectively enhanced by the electron−phonon coupling among the very huge number of Raman-active vibrations predicted by the optical selection rules for **TETCN4**, and they are actually recorded with a weak or very weak intensity.

Solid-state Raman spectra of different α,α′-end-capped sexithiophenes in various p-doped forms (i.e., radical cations, dications, and so on) have previously been reported.[13] The Raman spectral profile common to all of the dicationic species collected so far consists of a strong band near 1420−1415 cm^{-1} and another three medium-weak lines at 1220, 1160, and 1050 cm^{-1}. The peak positions and relative intensities of the Raman spectral fingerprints of the "doubly charged defects" are found to be quite similar to those recorded here for the main Raman features of the heteroquinoid **TETCN4** trimer. This close resemblance gives further support to the hypothesis that **TETCN4** can be viewed as a structural and electronic model of the dication or "positive bipolaron" species in p-doped aromatic oligothiophenes. Thus, the structural and electronic properties of the "charge carriers" should be more thoroughly explored by studying quinoid systems such as these thiophene-based quinodimethanes, which are completely free of chemical and conformational defects that are otherwise present in the doped polymer.

To finish, please let us call the attention of the reader to the observation of a shoulder at the high-energy side of the strongest Raman scattering at 1413 cm^{-1} in the solid-state spectrum of **TETCN4**. This feature, which results in being the second strongest Raman band, is not however predicted by the DFT//B3LYP/6-31G** calculations we have performed on a single molecule in the vacuum. The enlarged profile of the FT-Raman spectrum of solid **TETCN4** depicted in Figure 13 illustrates how this scattering at 1422 cm^{-1} and those assigned in the preceding paragraphs are selectively enhanced by the electron−phonon coupling with respect to the very many Raman-active

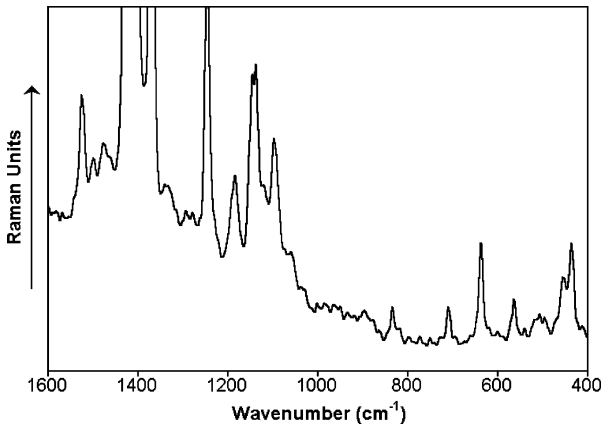

Figure 13. Enlarged profile of the solid-state FT-Raman spectrum of **TETCN4** showing the selective enhancement of particular skeletal ν(CC) stretching vibrations between 1500 and 1100 cm^{-1} with respect to the Raman scatterings recorded below 1000 cm^{-1}.

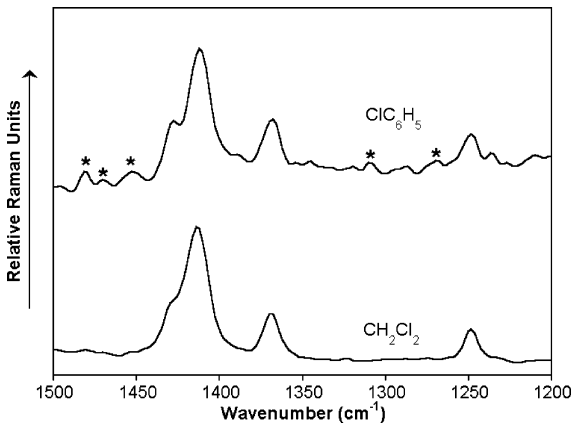

Figure 14. FT-Raman spectrum of **TETCN4** in dilute CH_2Cl_2 and C_6H_5Cl solutions in the 1500−1200 cm^{-1} Raman-shift spectral range (asterisks denote residual solvent scatterings).

vibrations recorded for this quinoidal trimer below 1000 cm^{-1}. Figure 14 displays the FT-Raman spectra of **TETCN4** in dilute CH_2Cl_2 and C_6H_5Cl solutions (after proper subtraction of the solvent scatterings). The whole Raman spectral profile of this oligothienyl quinodimethane does not show any drastic change upon solution of the solid sample, so that the molecule preserves its planarity in the liquid phase because of the rigidity of the π-conjugated backbone that prevents rotation around the thienyl units (nonetheless, the polarity of the solvent modifies somewhat the peak positions of the main Raman bands with respect to those of the pure solid). However, we observe that the "unexpected" Raman band at 1422 cm^{-1} loses intensity with respect to the main Raman line at 1413 cm^{-1} in going from the solid to the solutions. We believe it could be due to some sort of molecular aggregate affecting the π-conjugation properties (namely, π-stacking in the solid state or π-dimers in solution). In this regard, we observed some time ago a related phenomenon regarding the FT-Raman spectrum of the **T3CN4** quinoidal trimer: the strongest Raman bands recorded for the solid at 1428 and 1412 cm^{-1} were found to vary their peak positions and relative intensities upon heating of the sample or upon changing the power of the laser beam Raman excitation, thus suggesting a different origin for the two strongest Raman scatterings.[11b]

IV. Conclusions

We have reported on the synthesis of a novel thiophene-based quinodimethane bearing an electron-rich 3,4-ethylenedioxithio-

phene central unit. The molecular and electronic structures of this oligothienyl analogue of TCNQ have been investigated by UV−vis, infrared, and Raman spectroscopies and electrochemistry, together with DFT//B3LYP/6-31G** calculations. The π-conjugated backbone of this bis(dicyanomethylene)terthiophene exhibits a heteroquinoid-like pattern in the ground electronic state which results in being quite similar to that usually predicted for the dications or positive bipolarons of common aromatic oligothiophenes. The structural and electronic intervention of the EDO groups regarding the thienyl chain and the outermost electron-withdrawing groups has been analyzed as compared with other quinoidal homologues.

The heteroquinoid structure of **TETCN4** is characterized by a strong optical band near 680 nm, due to the HOMO → LUMO $S_0 \rightarrow S_1$ electronic transition. Theoretical calculations also show that this visible electromagnetic absorption meets its origin in the $\pi-\pi^*$ transition of the central terthienyl moiety and that no significant electron density is transferred toward the $=C(CN)_2$ end-caps upon such an excitation. Cyclic voltammetry results show that **TETCN4** displays a dual or amphoteric redox behavior. On one hand, it is easily reduced to the dianion due to the presence of the electron-withdrawing dicyanomethylene groups, likely leading to the full aromatization of the terthienyl backbone. On the other hand, it is also oxidized to the radical cation at an unexpected low potential. **TETCN4** could, therefore, act both as an electron-acceptor system or as an electron-donor system. This unusual behavior makes this novel **TETCN4** quinoidal trimer especially attractive for technological applications, since it might efficiently act as an n-type or p-type semiconductor in organic thin-film transistors.

The infrared and Raman spectra have also been comprehensively assigned on the basis of theoretical calculations. The strongest feature of both spectra corresponds to a ν(C═C)/ν(C−C) vibration spreading over the whole π-conjugated backbone. The Raman scattering at 1413 cm^{-1} has been assigned to the so-called ECC mode, which averages the collective in-phase motion of the whole sequence of polyconjugated C═C and C−C bonds, thus describing the evolution from the quinoid structure displayed by the molecule in its ground electronic state to an aromatic-like structure. The Raman spectral profile recorded for pristine **TETCN4** greatly resembles those previously collected for the dicationic species of many aromatic end-capped oligothiophenes, further supporting the similarities between the molecular and electronic structures of **TETCN4** and the "positive charge carriers" in thiophene-based π-conjugated systems. Finally, the differences evidenced in the Raman spectrum of this quinoidal trimer upon heating either the pure solid or the solution indicate that some of the strongest Raman scatterings (i.e., those mostly related to the π-electron degree of freedom) are sensitive to the molecular π-packing.

Acknowledgment. Research at the University of Málaga was supported by the Ministerio de Educación y Ciencia (MEC) of Spain through project BQU2003-05111 and by the Junta de Andalucía for funding our FQM-0159 scientific group. We are also indebted to MIUR-FIRB (Manipolazione molecolare per macchine nanometriche, project code RBNE019H9K) for financial support. M.C.R.D., R.P.O., and R.M.O. are also grateful to MEC and Junta de Andalucía for their personal doctoral grants. J.C. thanks the MEC for a Ramon y Cajal position of chemistry at the University of Malaga.

Supporting Information Available: Figures showing the B3LYP/6-31G** eigenvectors associated with selected IR- and Raman-active vibrations, respectively, of **TETCN4**. Scaled and experimental (in parentheses) wavenumbers are given in inverted centimeters. This material is available free of charge via the Internet at http://pubs.acs.org.

References and Notes

(1) (a) Inoue, Y.; Tokito, S.; Ito, K.; Suzuki, T. *J. Appl. Phys.* **2004**, *95*, 5795. (b) Horowitz, G. *J. Mater Res.* **2004**, *19*, 1946. (c) Sirringhaus, H. *Nat. Mater.* **2003**, *2*, 641. (d) Rogers, J. A.; Bao, Z.; Katz, H. E.; Dodabalapur, A. *Thin-Film Transistors*; Marcel Dekker: New York, 2003. (e) Dimitrakopoulos, C. D.; Malefant, P. R. L. *Adv. Mater.* **2002**, *14*, 99. (f) Malefant, P. R. L.; Dimitrakopoulos, C. D.; Gelorme, J. D.; Kosbar, L. L.; Graham, T. O.; Curioni, A.; Andreoni, W. *Appl. Phys. Lett.* **2002**, *80*, 2517.

(2) (a) Kunugi, Y.; Takimiya, K.; Toyoshima, Y.; Yamashita, K.; Aso, Y.; Otsubo, T. *J. Mater. Chem.* **2004**, *14*, 1367. (b) Facchetti, A.; Yoon, M.-H.; Stern, C. L.; Katz, H. E.; Marks, T. J. *Angew. Chem., Int. Ed.* **2003**, *42*, 3900. (c) Babel, A.; Janekhe, S. A. *J. Am. Chem. Soc.* **2003**, *125*, 13656. (d) Dodabalapur, A.; Lin, Y. Y.; Filas, R. W.; Bao, Z.; LaDuca, A.; Sarpeshkar, R.; Katz, H. E.; Li, W. *Nature* **2000**, *403*, 521.

(3) (a) Mas-Torent, M.; Hadley, P.; Bromley, S. T.; Ribas, X.; Tarres, J.; Mas, M.; Molins, E.; Veciana, J.; Rovira, C. *J. Am. Chem. Soc.* **2004**, *126*, 8546. (b) Sundar, V. C.; J.; Zaumseil, V. Podzorov; Menard, E.; Willett, R. L.; Someya, T.; Gershenson, M. E.; Rogers, J. A. *Science* **2004**, *303*, 1644. (c) Meng, H.; Bendikov, M.; Mitchell, G.; Holgeson, R.; Wudl, F.; Bao, Z.; Siegrist, T.; Kloc, C.; Chen, C.-H. *Adv. Mater.* **2003**, *15*, 1090.

(4) Sze, S. M. *Semiconductor Devices, Physics and Technology*; Wiley: New York, 1985.

(5) (a) Cornil, J.; Calbert, J. P.; Brédas, J. L. *J. Am. Chem. Soc.* **2001**, *123*, 1250. (b) Cornil, J.; Beljonne, D.; Calbert, J. P.; Brédas, J. L. *Adv. Mater.* **2001**, *13*, 1053. (c) Cornil, J.; Beljonne, D.; dos Santos, D. A.; Calbert, J. P.; Brédas, J. L. *Acc. Chem. Res.* **1999**, *32*, 267. (d) Cornil, J.; Calbert, J. P.; Beljonne, D.; Silbey, R.; Brédas, J. L. *Adv. Mater.* **2000**, *12*, 978.

(6) (a) Yui, K.; Aso, Y.; Otsubo, T.; Ogura, F. *J. Chem. Soc., Chem. Commun.* **1987**, 1816. (b) Yui, K.; Aso, Y.; Otsubo, T.; Ogura, F. *Bull. Chem. Soc. Jpn.* **1989**, *62*, 1539. (c) Yui, K.; Ishida, H.; Aso, Y.; Otsubo, T.; Ogura, F.; Kawamoto, A.; Tanaka, J. *Bull. Chem. Soc. Jpn.* **1989**, *62*, 1547. (d) Ishida, H.; Yui, K.; Aso, Y.; Otsubo, T.; Ogura, F. *Bull. Chem. Soc. Jpn.* **1990**, *63*, 2828. (e) Ogura, F.; Otsubo, T.; Aso, Y. *Sulfur Rep.* **1992**, *11*, 439. (f) Yoshida, S.; Fujii, M.; Aso, Y.; Otsubo, T.; Ogura, F. *J. Org. Chem.* **1994**, *59*, 3077. (g) Higuchi, H.; Nakayama, T.; Koyama, H.; Ojima, J.; Wada, T.; Sasabe, H. *Bull. Chem. Soc. Jpn.* **1995**, *68*, 2363. (h) Higuchi, H.; Yoshida, S.; Uraki, Y.; Ojima, J. *Bull. Chem. Soc. Jpn.* **1998**, *71*, 2229. (i) Casado, J.; Miller, L. L.; Mann, K. R.; Pappenfus, T. M.; Higuchi, H.; Orti, E.; Milian, B.; Pou-Amerigo, R.; Hernandez, V.; Lopez Navarrete, J. T. *J. Am. Chem. Soc.* **2002**, *124*, 12380.

(7) (a) Pappenfus, T. M.; Raff, J. D.; Hukkanen, E. J.; Burney, J. R.; Casado, J.; Drew, S. M.; Miller, L. L.; Mann, K. R. *J. Org. Chem.* **2002**, *67*, 6015. (b) Pappenfus, T. M.; Chesterfield, R. J.; Frisbie, C. D.; Mann, K. R.; Casado, J.; Raff, J. D.; Miller, L. L. *J. Am. Chem. Soc.* **2002**, *124*, 4184. (c) Chesterfield, R. J.; Newman, C. R.; Pappenfus, T. M.; Ewbank, P. C.; Haukaas, M. H.; Mann, K. R.; Miller, L. L.; Frisbie, C. D. *Adv. Mater.* **2003**, *15*, 1278.

(8) (a) Kunugi, Y.; Takimiya, K.; Toyoshima, Y.; Yamashita, K.; Aso, Y.; Otsubo, T. *J. Mater. Chem.* **2004**, *14*, 1367. (b) Yoon, M.-H.; DiBenedetto, S. A.; Facchetti, A.; Marks, T. J. *J. Am. Chem. Soc.* **2005**, *127*, 1348. (c) Sakamoto, Y.; Suzuki, T.; Kobayashi, M.; Gao, Y.; Fukai, Y.; Inoue, Y.; Sato, F.; Tokito, S. *J. Am. Chem. Soc.* **2004**, *126*, 8138.

(9) Janzen, D. E.; Burand, M. W.; Ewbank, P. C.; Pappenfus, T. M.; Higuchi, H.; da Silva Filho, D. A.; Young, V. G.; Brèdas, J.-L.; Mann, K. R. *J. Am. Chem. Soc.* **2004**, *126*, 15295.

(10) (a) Castiglioni, C.; López Navarrete, J. T.; Gussoni, M.; Zerbi, G. *Solid State Commun.* **1988**, *65*, 625. (b) Zerbi, G.; Castiglioni, C.; López Navarrete, J. T.; Tian, B.; Gussoni, M. *Synth. Met.* **1989**, *28*, D359. (c) Zerbi, G.; Gussoni, M.; Castiglioni, C. *Conjugated Polymers*; Kluwer Academic Publishers: Dordrecht, The Netherlands, 1991. (d) Agosti, E.; Rivola, M.; Hernández, V.; Del Zoppo, M.; Zerbi, G. *Synth. Met.* **1999**, *100*, 101.

(11) (a) Hernández, V.; Casado, J.; Ramírez, F. J.; Zotti, G.; Hotta, S.; López Navarrete, J. T. *J. Chem. Phys.* **1996**, *104*, 9271. (b) Hernández, V.; Hotta, S.; López Navarrete, J. T. *J. Chem. Phys.* **1998**, *109*, 2543. (c) Hernández, V.; Calvo Losada, S.; Casado, J.; Higuchi, H.; López Navarrete, J. T. *J. Phys. Chem. A* **2000**, *104*, 661. Casado, J.; Pappenfus, T. M.; Mann, K. R.; Ortí, E.; Viruela, P. M.; Milián, B.; Hernández, V.; López Navarrete, J. T. *ChemPhysChem* **2004** *5*, 529.

(12) (a) Casado, J.; Hotta, S.; Hernández, V.; López Navarrete, J. T. *J. Phys. Chem. A* **1999**, *103*, 816. (b) Hernández, V.; Casado, J.; Ramírez, F. J.; Alemany, L. J.; Hotta, S.; López Navarrete, J. T. *J. Phys. Chem.* **1996**, *100*, 289. (c) Hernández, V.; Muguruma, H.; Hotta, S.; López Navarrete, J. T. *J. Phys. Chem. A* **2000**, *104*, 735. (d) Casado, J.; Hernández, V.; Hotta, S.; López Navarrete, J. T. *J. Chem. Phys.* **1998**, *109*, 10419.

(13) (a) Casado, J.; Hernández, V.; Hotta, S.; López Navarrete, J. T. *Adv. Mater*. **1998**, *10*, 1458. (b) Casado, J.; Katz, H. E.; Hernández, V.; López Navarrete, J. T. *J. Phys. Chem. B* **2002**, *106*, 2488. (c) Casado, J.; Miller, L. L.; Mann, K. R.; Pappenfus, T. M.; Hernández, V.; López Navarrete, J. T. *J. Phys. Chem. B* **2002**, *106*, 3597.

(14) Zhu, Y.; Wolf, M. O. *J. Am. Chem Soc.* **2000**, *122*, 10121.

(15) Frisch, M. J.; Trucks, G. W.; Schlegel, H. B.; Scuseria, G. E.; Robb, M. A.; Cheeseman, J. R.; Montgomery, J. A., Jr.; Vreven, T.; Kudin, K. N.; Burant, J. C.; Millam, J. M.; Iyengar, S. S.; Tomasi, J.; Barone, V.; Mennucci, B.; Cossi, M.; Scalmani, G.; Rega, N.; Petersson, G. A.; Nakatsuji, H.; Hada, M.; Ehara, M.; Toyota, K.; Fukuda, R.; Hasegawa, J.; Ishida, M.; Nakajima, T.; Honda, Y.; Kitao, O.; Nakai, H.; Klene, M.; Li, X.; Knox, J. E.; Hratchian, H. P.; Cross, J. B.; Bakken, V.; Adamo, C.; Jaramillo, J.; Gomperts, R.; Stratmann, R. E.; Yazyev, O.; Austin, A. J.; Cammi, R.; Pomelli, C.; Ochterski, J. W.; Ayala, P. Y.; Morokuma, K.; Voth, G. A.; Salvador, P.; Dannenberg, J. J.; Zakrzewski, V. G.; Dapprich, S.; Daniels, A. D.; Strain, M. C.; Farkas, O.; Malick, D. K.; Rabuck, A. D.; Raghavachari, K.; Foresman, J. B.; Ortiz, J. V.; Cui, Q.; Baboul, A. G.; Clifford, S.; Cioslowski, J.; Stefanov, B. B.; Liu, G.; Liashenko, A.; Piskorz, P.; Komaromi, I.; Martin, R. L.; Fox, D. J.; Keith, T.; Al-Laham, M. A.; Peng, C. Y.; Nanayakkara, A.; Challacombe, M.; Gill, P. M. W.; Johnson, B.; Chen, W.; Wong, M. W.; Gonzalez, C.; Pople, J. A. *Gaussian 03*, revision A.1; Gaussian, Inc.: Wallingford, CT, 2004.

(16) Becke, A. D. *J. Chem. Phys.* **1993**, *98*, 1372.

(17) Francl, M. M.; Pietro, W. J.; Hehre, W. J.; Binkley, J. S.; Gordon, M. S.; Defrees, D. J.; Pople, J. A. *J. Chem. Phys*. **1982**, *77*, 3654.

(18) Portmann, S.; Lüthi, H. P. *Chimia* **2000**, *54*, 766.

(19) (a) Runge, E.; Gross, E. K. U. *Phys. Rev. Lett*. **1984**, *52*, 997. (b) Gross, E. K. U.; Kohn, W. *Adv. Quantum Chem.* **1990**, *21*, 255. (c) Gross, E. K. U.; Ullrich, C. A.; Gossman, U. J. *Density Functional Theory*; Plenum Press: New York, 1995.

(20) Casida, M. E. *Recent Advances in Density Functional Methods, Part I*; World Scientific: Singapore, 1995.

(21) Koch, W.; Holthausen, M. C. *A Chemist's Guide to Density Functional Theory*; Wiley-VCH: Weinheim, Germany, 2000.

(22) Hsu, C.-P.; Hirata, S.; Head-Gordon, M. *J. Phys. Chem. A* **2001**, *105*, 451.

(23) (a) Hirata, S.; Lee, T. J.; Head-Gordon, M. *J. Chem. Phys*. **1999**, *111*, 8904. (b) Heinze, H. H.; Görling, A.; Rösch, N. *J. Chem. Phys*. **2000**, *113*, 2088. (c) Weisman, J. L.; Lee, T. J.; Head-Gordon, M. *Spectrochim. Acta, Part A* **2001**, *57*, 931. (d) Hirata, S.; Head-Gordon, M.; Szcsepanski, J.; Vala, M. *J. Phys. Chem*. **2003**, *107*, 4940. (e) Grimme, S.; Parac, M. *ChemPhysChem* **2003**, *3*, 292. (f) Parac, M.; Grimme, S. *Chem. Phys.* **2003**, *292*, 11.

(24) Halasinski, T. M.; Weisman, J. L.; Ruiterkamp, R.; Lee, T. J.; Salama, F.; Head-Gordon, M. *J. Phys. Chem. A* **2003**, *107*, 3660.

(25) Bauernschmitt, R.; Ahlrichs, R.; Heinrich, F. H.; Kappes, M. M. *J. Am. Chem. Soc.* **1998**, *120*, 5052.

(26) (a) Pogantsch, A.; Heimel, G.; Zojer, E. *J. Chem. Phys.* **2002**, *117*, 5921. (b) Hutchison, G. R.; Ratner, M. A.; Marks, T. J. *J. Phys. Chem. A* **2002**, *106*, 10596. (c) Casado, J.; Pappenfus, T. M.; Miller, L. L.; Mann, K. R.; Ortí, E.; Viruela, P. M.; Pou-Amérigo, R.; Hernández, V.; López Navarrete, J. T. *J. Am. Chem. Soc.* **2003**, *125*, 2524.

(27) (a) van Gisbergen, S. J. A.; Rosa, A.; Ricciardi, G.; Baerends, E. J. *J. Chem. Phys*. **1999**, *111*, 2499. (b) Nguyen, K. A.; Pachter, R. *J. Chem. Phys*. **2001**, *114*, 10757. (c) Jaworska, M.; Kazibut, G.; Lodowski, P. *J. Phys. Chem. A* **2003**, *107*, 1339.

(28) Yamaguchi, Y. *J. Chem. Phys*. **2002**, *117*, 9668.

(29) Pou-Amérigo, R.; Viruela, P. M.; Viruela, R.; Rubio, M.; Ortí, E. *Chem. Phys. Lett.* **2002**, *352*, 491.

(30) Scott, A. P.; Radom, L. *J. Phys. Chem*. **1996**, *100*, 16502.

(31) Hotta, S.; Waragai, K. *J. Mater. Chem*. **1991**, *1*, 835.

(32) Graf, D. D.; Duan, R. G.; Campbell, J. P.; Miller, L. L.; Mann, K. R. *J. Am. Chem. Soc.* **1997**, *119*, 5888.

(33) Graf, D. D.; Campbell, J. P.; Mann, K. R.; Miller, L. L. *J. Am. Chem. Soc.* **1996**, *118*, 5480.

(34) (a) Alemán, C.; Juliá, L. *J. Phys. Chem.* **1996**, *100*, 14661. (b) Irle, S.; Lischka, H. *J. Chem. Phys.* **1997**, *107*, 3021. (c) Moro, G.; Scalmani, G.; Cossentino, U.; Pitea, D. *Synth. Met.* **1998**, *92*, 69.

(35) van Pham, C.; Burkhardt, A.; Shabana, R.; Cunningham, D. D.; Mark, H. B.; Zimmer, H. *Phosphorus, Sulfur Silicon Relat. Elem.* **1989**, *46*, 153.

(36) Casado, J.; Ponce Ortiz, R.; Ruiz Delgado, M. C.; Azumi, R.; Oakley, R. T.; Hernández, V.; López Navarrete, J. T. *J. Phys. Chem. B* **2005**, *109*, 10115.

(37) Tozer, D. A.; Amos, R. D.; Handy, N. C.; Roos, B. O.; Serrano-Andrés, L. *Mol. Phys.* **1999**, *97*, 859.

(38) (a) Jamorski, C.; Foresman, J. B.; Thilgen, C.; Lüthi, H.-P. *J. Chem. Phys.* **2002**, *116*, 8761. (b) Jamorski, C.; Lüthi, H.-P. *J. Chem. Phys.* **2002**, *117*, 4146 and 4157.

(39) (a) Hotta, S.; Waragai, K. *J. Phys. Chem*. **1993**, *97*, 7427. (b) Gebauer, W.; Sokolowski, M.; Umbach, E. *Chem. Phys.* **1998**, *227*, 33. (c) Gierschner, J.; Mack, H.-G.; Egelheaf, H.-J.; Schweizer, S.; Doser, B.; Oelkrug, D. *Synth. Met.* **2003**, *138*, 311.

(40) Yui, K.; Aso, Y.; Otsubo, T.; Ogura, F. *Bull. Chem. Soc. Jpn.* **1989**, *62*, 1539.

(41) (a) Baüerle, P.; Segelbacher, U.; Maier, A.; Mehring, M. *J. Am. Chem. Soc*. **1993**, *115*, 10217. (b) Baüerle, P.; Segelbacher, U.; Gaudl, K. U.; Huttenlocher, D.; Mehring, M. *Angew. Chem., Int. Ed. Engl*. **1993**, *32*, 76.

(42) Diaz, A. F.; Crowley, J.; Bargon, J.; Gardini, G. P.; Torrance, J. B. *J. Electroanal. Chem*. **1981**, *121*, 355.

(43) Chapell, J. S.; Bloch, A. N.; Bryden, W. A.; Maxfield, M.; Poehler, T. O.; Cowan, D. O. *J. Am. Chem. Soc*. **1981**, *103*, 2442.

(44) (a) Takenaka, T. *Spectrochim. Acta, Part A* **1971**, *27*, 1735. (b) Girlando, A.; Pecile, C. *Spectrochim. Acta, Part A* **1973**, *29*, 1859. (c) Faulques, E.; Leblanc, A.; Molini, P.; Decoster, M.; Conan, F.; Guerchais, J. E.; Sala-Sala, J. *Spectrochim. Acta, Part A* **1995**, *51*, 805.

(45) Khathake, M. S.; Devlin, J. P. *J. Chem. Phys.* **1979**, *70*, 1851.

(46) Hernández, V.; Castiglioni, C.; Del Zoppo, M.; Zerbi, G. *Phys. Rev. B* **1994**, *50*, 9815.

(47) Horovitz, B. *Phys. Rev. Lett*. **1981**, *47*, 1491.

(48) Casado, J.; Hernández, V.; Ruiz Delgado, M. C.; Ponce Ortiz, R.; López Navarrete, J. T.; Facchetti, A.; Marks, T. J. *J. Am. Chem. Soc*. **2005**, *127*, 13364.